Hydro-Mechanical Model of Electro-Hydraulic Servovalve Based on Bond Graph

Yaozhong Xu, Eric Bideaux, Sylvie Sesmat, Lilia Sidhom, Xavier Brun

▶ **To cite this version:**

Yaozhong Xu, Eric Bideaux, Sylvie Sesmat, Lilia Sidhom, Xavier Brun. Hydro-Mechanical Model of Electro-Hydraulic Servovalve Based on Bond Graph. 6th Fluid Power Net International PhD Symposium, Jul 2010, West Lafayette, United States. hal-00988577

HAL Id: hal-00988577

https://hal.science/hal-00988577v1

Submitted on 30 Apr 2019

HAL is a multi-disciplinary open access archive for the deposit and dissemination of scientific research documents, whether they are published or not. The documents may come from teaching and research institutions in France or abroad, or from public or private research centers.

L'archive ouverte pluridisciplinaire **HAL**, est destinée au dépôt et à la diffusion de documents scientifiques de niveau recherche, publiés ou non, émanant des établissements d'enseignement et de recherche français ou étrangers, des laboratoires publics ou privés.

HYDRO-MECHANICAL MODEL OF ELETRO-HYDRAULIC SERVOVALVE BASED ON BOND GRAPH

Yaozhong XU[1], Eric BIDEAUX[2], Sylvie SESMAT[2], Lilia SIDHOM[1], and Xavier BRUN[2]
Université de Lyon, Institut National des Sciences Appliquées de LYON
Laboratoire Ampère, UMR CNRS 5005
25 avenue Jean Capelle
69621 Villeurbanne Cedex
France
Email: yaozhong.xu@insa-lyon.fr

Bond Graph, as a graphical modeling language, can represent various physical domains in a unified form. This paper deals with the establishment of a Bond Graph model of an electro-hydraulic servovalve which consists of a torque motor, a cantilever feedback spring, and two hydraulic stages, one with a nozzle/flapper system and the other with a spool valve. The entire model can be divided into a hydraulic and a mechanical part which are connected by 2-port modulated R-elements representing orifice pressure drop and jet force phenomena, and TF-elements coupling the mechanical and hydraulic power. The Bond Graph model of whole system is then presented. Finally, using AMESim on which a model was created based on the established Bond Graph, simulation results are compared with the experimental measurements.

Keywords: Bond Graph, Electro-hydraulic servovalve, Dynamic model, Simulation

1 INTRODUCTION

An electro-hydraulic servovalve is a servomechanism that constitutes the main interface between the electrical control signal and the fluid power actuator. When large flow rates are required, two-stage servovalves are usually employed. It mainly consists of a main spool valve, a nozzle/flapper pilot valve, a feedback spring and a torque motor as shown in Fig. 1. The electric command, generated by an integrated spool position controller, is applied to the torque motor for deflecting the nozzle/flapper system; this produces a pressure difference across the drive areas of the spool and induces its movement. The spool displacement and the flapper deflection create a bend of the feedback spring, which results in a force across the flapper that is fed back to the pilot torque. At the same time, the spool displacement leads to control the output flow rates according to the electric control signal. The studied servovalve, a MOOG D765, can provide a quite large bandwidth, thus a short response time, and a good precision. As indicated in the MOOG technical bulletin, the bandwidth reaches more than 500 Hz for 5% of spool displacement with a rated flow up to 19 l/min at 70 bar pressure drop and full opening.

As the servovalve takes a crucial place at the electro-hydraulic interface of systems, the analysis of servovalve dynamics becomes a essential point in electro-hydraulic control system design, as well as in servovalve design (**Yuan Q.H.; Li P.Y.** (2002); **Kang, R.J.; Jiao, Z.X.; Mare J.C.; Shang, Y.X.; Wu, S.** (2009)). However, the problem is troublesome due to the multidisciplinary nature of

[1] PhD candidate
[2] Supervisor

this type of component that requires electric, mechanical and hydraulic knowledge. Many researchers tend to analyze and design the control of servovalves by linearizing the nonlinear state equations to reformulate the problem with high-order linear models. **Watton, J.** (1987) engages most efforts into the dynamics of the nozzle/flapper pilot valve and then proposes a 4th order model. Others authors taking into account more details about the servovalve have developed more accurate but higher-order models, e.g. **Kim, D.H.; Tsao, T.-C.** (2000) have formulated a 5th order model considering the compressibility of fluid in the pilot valve chambers. Although all of these linearized models are derived from the nonlinear state equations, and hence their coefficients can be partially expressed in terms of valve physical parameters and fluid properties, they are usually only valid for a specific frequency range at a given spool displacement and their parameters have to be adjusted if the spool displacement changes. These linear approaches are adequate for most of the conventional applications at low frequency, but if we want to fully exploit the high performances of servovalves such as the MOOG D765, it is necessary to develop a servovalve model which is accurate simultaneously on a wide range of spool displacement and frequency. Moreover, the study of the servovalve behavior at high frequency involves new phenomena that are highly influencing the servovalve performances, and therefore, the energy exchanges among the physical components have to be even more carefully represented (**Rabie, G.; Lebrun, M.** (1981); **Maré, J.C.** (1996)).

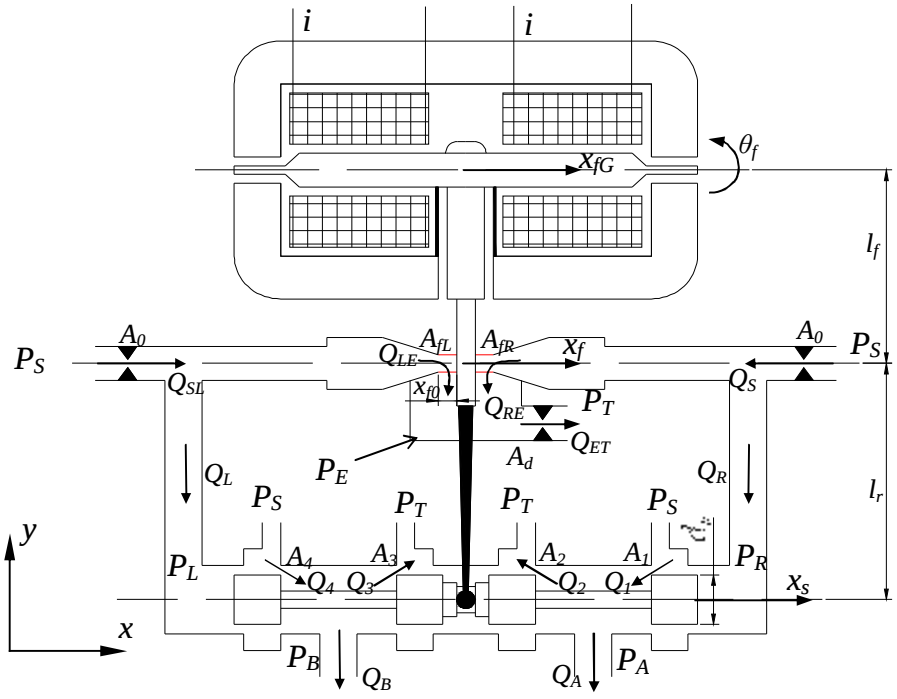

Fig. 1: Two-stage electro-hydraulic servovalve configuration

The Bond Graph (**Karnopp, D.C.; Rosenberg, R.C.** (1975)) shows an excellent capacity to deal with this kind of problems (**Karnopp, D.** (1972); **Dransfield, P.; Teo, M.K.** (1979); **Suzuki, K.; Nakamura, I.; Thoma, J.U.** (1999)). After establishment of the main architecture of the system model by Bond Graph, this methodology enables engineers to refine the model by adding or removing graphically some phenomena without having to start again the whole modeling phase. It provides a useful and convenient method for analyzing complex systems which are concerned with multidiscipline and whose models usually need to be modified. Besides, it can be used to study the system structural properties (observability, controllability, etc.) thanks to causal analysis.

This paper intends to analyze the dynamic characteristics of a two-stage electro-hydraulic servovalve by Bond Graph. The organization of the paper is as follows: Sections II and III aim to establish Bond Graph model for hydraulic and mechanical parts of nozzle/flapper system and spool valve. Section IV will deal with the model of the entire system and implementation of simulation.

2 DYNAMICS MODELS OF THE NOZZLE/FLAPPER SYSTEM

2.1 Bond Graph of hydraulic model of the nozzle/flapper system

Considering flows in the nozzle/flapper stage (see in Fig. 1), note that the flows through fix orifices and nozzles can be given by the orifice flow equation as (**Merritt, H.E.** (1967)):

$$Q_{SL} = A_0 C_{d0} \sqrt{\frac{2}{r}(P_S - P_L)} = \frac{p}{4} d_0^2 C_{d0} \sqrt{\frac{2}{r}(P_S - P_L)} \tag{1}$$

$$Q_{SR} = A_0 C_{d0} \sqrt{\frac{2}{r}(P_S - P_R)} = \frac{p}{4} d_0^2 C_{d0} \sqrt{\frac{2}{r}(P_S - P_R)} \tag{2}$$

$$Q_{LE} = A_{fL} C_{df} \sqrt{\frac{2}{r}(P_L - P_E)} = p d_n (x_{f0} + x_f) \cdot C_{df} \sqrt{\frac{2}{r}(P_L - P_E)} \tag{3}$$

$$Q_{RE} = A_{fR} C_{df} \sqrt{\frac{2}{r}(P_R - P_E)} = p d_n (x_{f0} - x_f) \cdot C_{df} \sqrt{\frac{2}{r}(P_R - P_E)} \tag{4}$$

$$Q_{ET} = Q_{LE} + Q_{RE} = A_d C_{dd} \sqrt{\frac{2}{r}(P_E - P_T)} = \frac{p}{4} d_d^2 C_{dd} \sqrt{\frac{2}{r}(P_E - P_T)} \tag{5}$$

Taking into account the compressibility of fluid in each chamber of the nozzle/flapper system, the pilot flows injected into the main spool valve for driving its movement are expressed as follows:

$$Q_L = Q_{SL} - Q_{LE} = \frac{1}{b} V_L \frac{dP_L}{dt} + A_s \frac{dx_s}{dt} \tag{6}$$

$$Q_R = Q_{SR} - Q_{RE} = \frac{1}{b} V_R \frac{dP_R}{dt} - A_s \frac{dx_s}{dt} \tag{7}$$

To represent this compressibility effect in Bond Graph, a convenient means is the use of a 2-port capacitive phenomenon which couples hydraulic and mechanical behaviors (**Karnopp, D.C.; Rosenberg, R.C.** (1975)). Besides, all of the orifice flows can be expressed by resistive phenomena in Bond Graph due to power dissipation due to pressure drop. The Bond Graph of the hydraulic part of the nozzle/flapper system is then shown in Fig. 2.

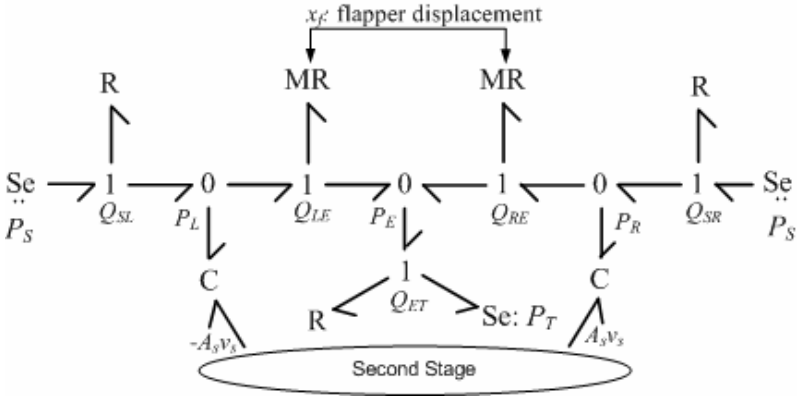

Fig. 2: Bond Graph of the hydraulic part of the nozzle/flapper system

2.2 Bond Graph of mechanical model of the flapper/armature

The first-stage flapper is influenced by the following forces (**Morse, A.C.** (1963)): (1) control force which is derived from the torque motor and proportional to the input electrical current, (2) spring force proportional to the deflection of the cantilever feedback spring, (3) flexible tube force caused by the deflection of the flexible tube, (4) hydrostatic force produced by the pressure difference applied on the two sides of the flapper, (5) hydrodynamic force due to the nonuniform pressure distribution caused by the fluid flow across the areas between nozzles/flapper, and (6) viscous damping force due to mechanical armature mounting and load. Models for the reaction of the feedback spring and flexible tube can be developed from the mechanics of materials. Thus, the resultants of forces and torques that act on the center of gravity of the entire flapper/armature are given as:

$$m_f \frac{d^2 x_{fG}}{dt^2} = 3K_r \cdot x_r - \left(6l_t \cdot K_t \cdot q_f + 12K_t \cdot x_{fG}\right) + F_{fhs} + F_{fhd} \tag{8}$$

$$J_f \frac{d^2 q_f}{dt^2} = K_m i + 3K_r \cdot x_r \cdot \left(l_f + l_r\right) - \left(4l_t^2 \cdot K_t \cdot q_f + 6l_t \cdot K_t \cdot x_{fG}\right) + \left(F_{fhs} + F_{fhd}\right) \cdot l_f - B_f \frac{dq_f}{dt} \tag{9}$$

where symbols are defined as:

$K_t = \frac{E_t I_t}{l_t^3}$ and $K_r = \frac{E_r I_r}{l_r^3}$ are flexible tube constant and feedback spring constant;

$F_{fhs} = \left(P_L - P_R\right) \cdot \frac{p d_n^2}{4}$ is the hydrostatic force;

$F_{fhd} = \frac{4r}{p d_n^2}\left(Q_{LE}^2 - Q_{RE}^2\right)$ is the hydrodynamic force.

Note that the modal frequencies of translational vibration are quite higher than those of rotational one (**Maré, J.C.** (1996)). The mass of the flapper/armature then can be neglected. Eq. (8) and (9) are reduced to one equation concerning the rotational dynamics of the system which is written as:

$$J_f \frac{d^2 q_f}{dt^2} = K_m i + 3K_r \cdot x_r \cdot l_{re} - l_t^2 \cdot K_t \cdot q_f + \left(F_{fhs} + F_{fhd}\right) \cdot l_{fe} - B_f \frac{dq_f}{dt} \tag{10}$$

where $l_{re} = l_f + l_r - \frac{l_t}{2}$, $l_{fe} = l_f - \frac{l_t}{2}$, and $x_r = x_s - l_{re} \cdot q_f$.

According to Eq. (10), the Bond Graph of the mechanical part of the flapper/armature is presented in Fig. 3.

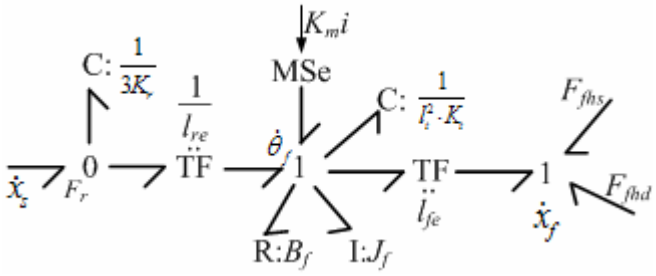

Fig. 3: Bond Graph of the mechanical part of the flapper/armature

3 DYNAMICS MODELS OF THE SPOOL VALVE

3.1 Bond Graph of hydraulic model of the spool valve

For flow calculation in the spool valve, note that local geometric defects influence significantly the flow evolution. In order to take into account these effects, the local geometry of the spool is defined as shown in Fig. 4.

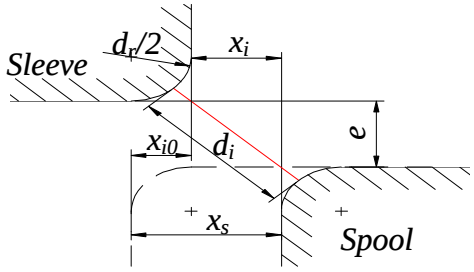

Fig. 4: Local geometric configuration around spool and valve control port

According to Fig. 4, the opening diameter is given by:

$$d_i = \begin{cases} \sqrt{(e+d_r)^2 + (d_r + x_i)^2} - d_r & if \quad x_i \geq -d_r \\ e & if \quad x_i < -d_r \end{cases} \tag{11}$$

where

$$x_i = \begin{cases} x_s - x_{i0} & i = 1,3 \\ -x_s - x_{i0} & i = 2,4 \end{cases} \tag{12}$$

Let us define the initial opening as:

$$d_0 = d_i(0) = \sqrt{(e+d_r)^2 + d_r^{\,2}} - d_r \tag{13}$$

The flows in spool valve can be defined as two types of flows: (1) orifice flow when $x_i \geq 0$ and (2) leakage flow when $x_i < 0$. The orifice flow in the underlap position ($x_i \geq 0$) is evaluated by (**Merritt, H.E.** (1967)):

$$Q_{i,underlap} = C_{di} A_i \sqrt{\frac{2}{r}|\Delta P|} = C_{di} p d_s d_i \sqrt{\frac{2}{r}|\Delta P|} \quad if \;\; x_i \geq 0 \tag{14}$$

where ΔP is the pressure drop corresponding to the valve control port;

C_{di} is the flow coefficient derived from asymptotes of $C_d - \sqrt{\mathrm{Re}}$ curves,

and $C_{di} = \begin{cases} d\sqrt{\mathrm{Re}_i} & if \quad \mathrm{Re}_i < \mathrm{Re}_t \\ C_{di,\infty} & if \quad \mathrm{Re}_i \geq \mathrm{Re}_t \end{cases}$

with $\mathrm{Re}_i = \dfrac{r \cdot Q_i \cdot 2d_i}{m \cdot A_i} = \dfrac{2r \cdot Q_i}{m \cdot p d_s}$ and $\mathrm{Re}_t = \left(\dfrac{C_{di,\infty}}{d} \right)^2$.

In an overlap position ($x_i < 0$), note that when $x_i >> e$ the flow complies with the law of Hagen-Poiseuille. That is, in this case, the flow is inversely proportional to the overlap length. In practice, there exists a transitional region along with the spool displacement. In this region, the additional kinetic energy losses consist of those due to fluid inertia for the acceleration in transition length, and entrance and exit ones. The leakage flow between the spool and the sleeve valve can be expressed with replacement by an equivalent overlap length as:

$$Q_{i,overlap} = \frac{pd_s e^3}{12m \cdot \left(x_0 - x_i + k_I \tanh\left(-\frac{x_i}{L_t} \right) \right)} |\Delta P| \quad if \ x_i < 0 \tag{15}$$

In the expression of equivalent overlap length, the first term x_0 accounts for the entrance and exit losses. The losses due to fluid inertia are taken into account in the third term accounts in which L_t represents the transition length.

Let's consider the conditions to define smooth flow curves, that is

$$\lim_{x_i \to 0} Q_{i,underlap} = \lim_{x_i \to 0} Q_{i,overlap} \text{ and } \lim_{x_i \to 0} Q'_{i,underlap} = \lim_{x_i \to 0} Q'_{i,overlap} \tag{16}$$

Assuming that $L_t = k_t d_0$, the unknown parameters can be given by:

$$x_0 = \frac{e^3}{48d^2 \cdot d_0^2} \tag{17}$$

$$k_I = k_t \left(2 \cdot x_0 \cdot d_i'(0) - d_0 \right) = k_t \cdot \left(\frac{e^3 \cdot d_r}{24d^2 \cdot d_0^2 (d_0 + d_r)} - d_0 \right) \tag{18}$$

The flow rates at the control ports A and B are expressed as:

$$Q_A = Q_1 - Q_2 \text{ and } Q_B = Q_3 - Q_4 \tag{19}$$

While applying modulated R-element to represent the valve resistance to the flows, the Bond Graph of the hydraulic part of the spool valve is given in Fig. 5.

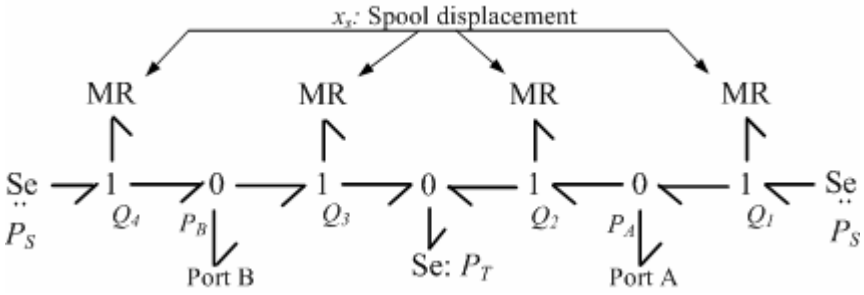

Fig. 5: Bond Graph of the hydraulic part of the spool valve

3.2 Bond Graph of mechanical model of the spool

The forces acting upon the second-stage spool include the following types (**Morse, A.C.** (1963)): (1) pilot force due to a difference pressure across the spool produced by the pilot stage, (2) spring force proportional to the deflection of the cantilever feedback spring, (3) hydrodynamic force due to the nonuniform pressure distribution caused by the flow across the valve control ports, and (4) frictional force between spool/sleeve with a viscous friction coefficient assumed to be constant. The resultants of forces applied to the spool are given as:

$$m_s \frac{d^2 x_s}{dt^2} = \frac{pd_s^2}{4} \cdot (P_L - P_R) - 3K_r \cdot x_r - B_s \frac{dx_s}{dt} + F_{shd} \tag{20}$$

where the spool hydrodynamic force $F_{shd} = r \cdot \left(\frac{\cos q_2}{A_2} Q_2^2 - \frac{\cos q_1}{A_1} Q_1^2 + \frac{\cos q_4}{A_4} Q_4^2 - \frac{\cos q_3}{A_3} Q_3^2 \right)$ with θ_i evaluated by Eq. (21) (**Merritt, H.E.** (1967)).

$$\frac{x_i}{e} = \frac{1+\frac{p}{2}\sin(q_i) - \ln\left(tg\frac{1}{2}(p-q_i)\right)\cdot\cos(q_i)}{1+\frac{p}{2}\cos(q_i) + \ln\left(tg\frac{1}{2}(p-q_i)\right)\cdot\sin(q_i)} \tag{21}$$

Fig. 6 has shown the Bond Graph of the mechanical part of the spool by applying a 1-junction for the spool motion.

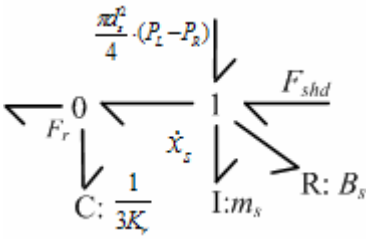

Fig. 6: Bond Graph of the mechanical part of the spool

4 BOND GRAPH OF THE ENTIRE SYSTEM AND SIMULATION RESULT

To properly model the coupling between the hydraulic and mechanical parts, 2-port R-elements modulated by the spool or flapper displacement are used for representing the pressure drop at one port and the hydraulic jet force at the other. Besides, TF-elements are used for modelling the conversion between hydraulic and mechanical power. In addition, the system contains an electric feedback corresponding to the spool position measurement. Bond Graph of the entire system is finally shown in Fig. 7.

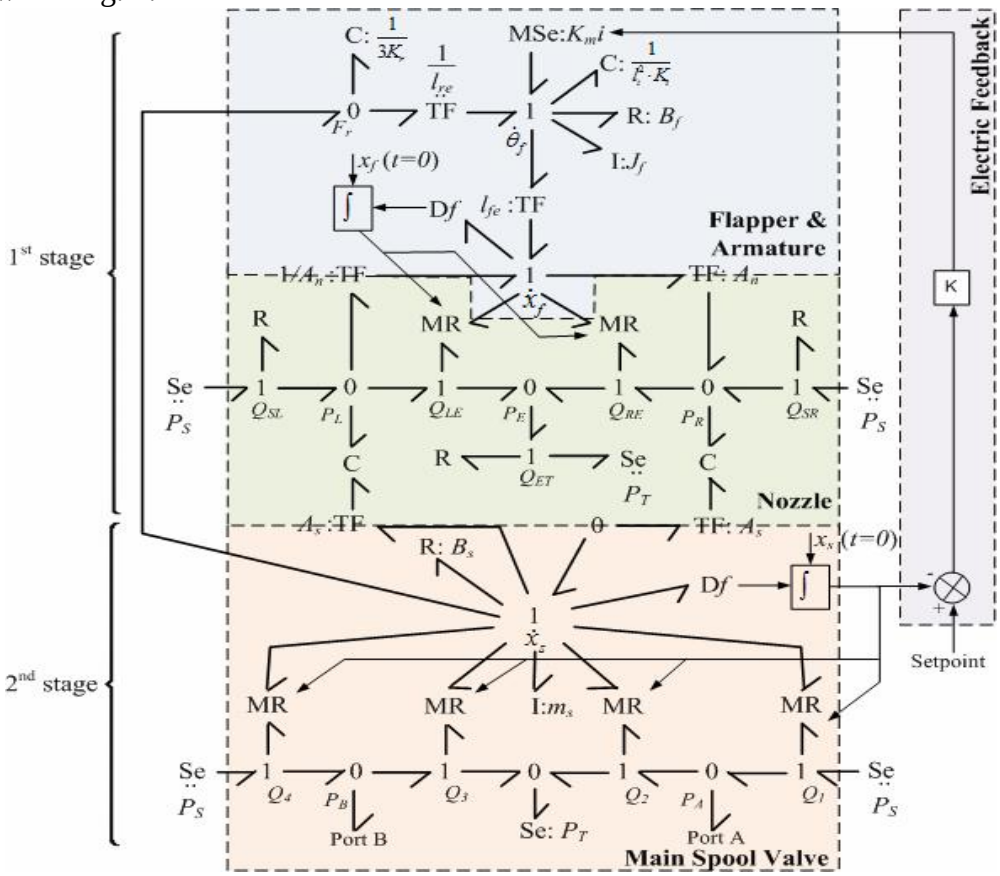

Fig. 7: Bond Graph model of the entire system

The tested servovalve is a MOOG D765-D128 servovalve delivering a 19 l/min rated flow at 70 bar valve pressure drop and 10 V corresponding to the maximum spool displacement. The Levenberg-

Marquardt method is applied to estimate the unknown parameters in flow equations (11) and (12) using the leakage experimental characteristic of the servovalve. The simulated leakage flow curve is compared to the experimental results in Fig. 8, and it shows that the use of the identified parameters in Eq. (11) and (12) for simulation can efficiently represent the real leakage characteristic. The result of leakage simulation in Fig. 8 fits well with the experiment, the average error is less than 0.008 l/min and the maximum error equal to 0.03 l/min.

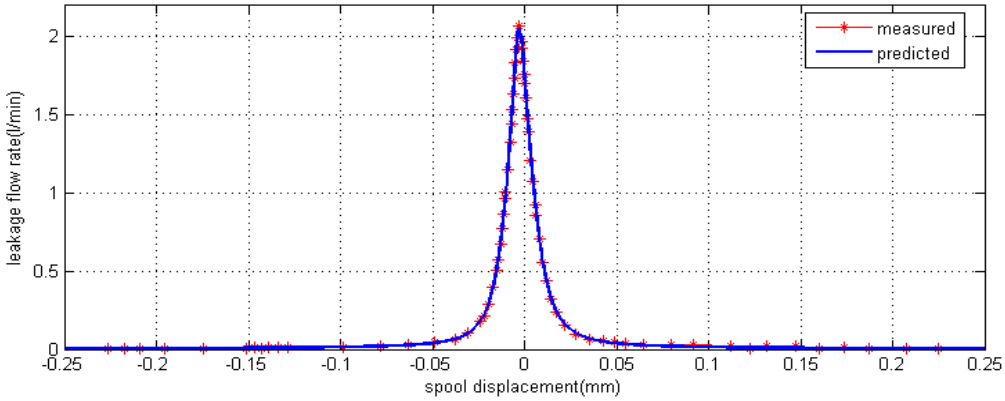

Fig. 8: Leakage flow: experiment and simulation

Using these identified parameters in the complete model, the servovalve responses has been computed for sinusoidal signals at ±40% and ±100% of the maximum input and on a frequency range between 1 and 500 Hz. The spool position magnitude and the phase lags corresponding to each sinusoidal input have also been measured. The comparison between experimental results and simulation is shown in Fig. 9.

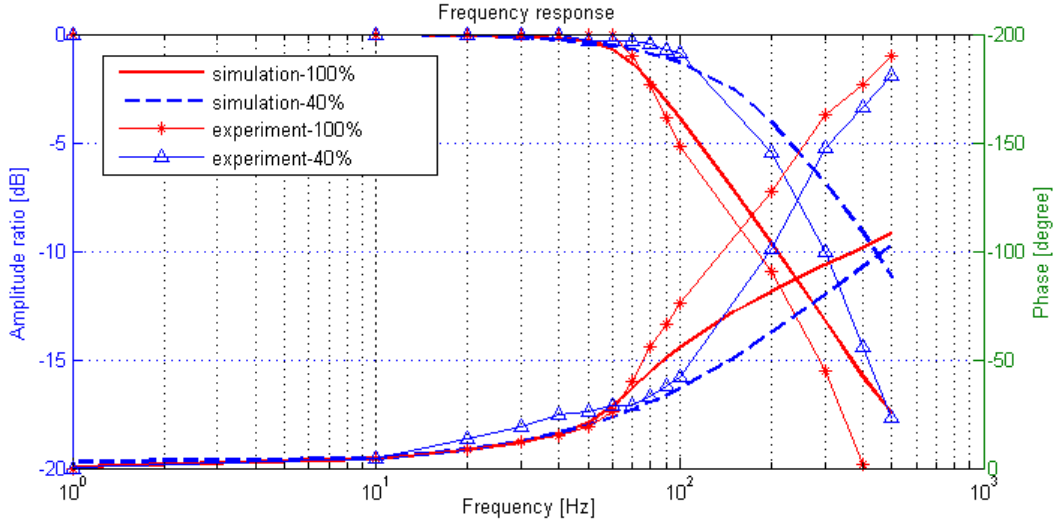

Fig. 9: Frequency response: experiment and simulation

For the dynamic characteristics, we can note that the simulated amplitude ratio and phase (see in Fig. 9) show also a good agreement with the experimental result at low frequency. However, a larger error is observed at high frequency, especially for the phase. This could be explained since we have neglected the influence of high frequency vibration mode of the flapper, and the difference between simulation and experiment became more important with the increase of frequency. In addition, the model has been established without considering the dynamics of the torque motor (especially the electromagnetic hysteresis), which results at high frequency (500 Hz) in a significant phase error over 80° and a amplitude ratio error larger than 6 dB. Nevertheless, the dynamic model is valid until 100Hz where the phase error is less than 6° and amplitude ratio error less than 0.5 dB for 40% of input signal.

5 CONCLUSION

The electro-hydraulic servovalve, as a multidisciplinary servomechanism, is complex and it is difficult to build up a dynamic model which can be expressed only by parameters derived from the physical components. Along with the establishment of the Bond Graph model of the MOOG D765 servovalve, we show that an accurate model for a large range of frequency and spool displacement can be obtained with a fully physical approach, that is the knowledge of all relevant constitutive equations and physical parameters. Besides, with a clear graphical architecture, the developed Bond Graph model can now be conveniently analyzed in regards with the system physical parameters, as well as improved by adding new phenomena when further effects are taken into consideration.

6 LIST OF NOTATIONS

$Q_{SL(R)}$	Upstream orifice flow rates of the nozzle/flapper system	m^3/s
$Q_{L(R)E}$	flow rates through nozzles	m^3/s
Q_E, $Q_{L(R)}$	Total drain orifice flow rate, pilot flow rates on left (right) side	m^3/s
$Q_{i,underlap}$, $Q_{i,overlap}$	Flow rates of orifice i of spool valve in underlap (overlap) position	m^3/s
$Q_{A(B)}$	Output flow rates	m^3/s
C_{di}, $C_{di,\infty}$	Flow coefficients of orifice i of spool valve, and those coefficients with a large valve opening	
C_{d0}, C_{df}, C_{dd}	Flow coefficients of upstream orifices, nozzles and drain orifice of the nozzle/flapper system	
A_0, $A_{fL(R)}$, A_d	Areas of upstream orifices, nozzles and drain orifice of the nozzle/flapper system	m^2
A_s	Spool area	m^2
d_0, d_n, d_d	Diameter of upstream orifices, nozzles and drain orifice of the nozzle/flapper system	m
d_r, d_i, d_0, d_s	Diameter of rounded edges, orifice i, initial orifice opening and spool	m
e	Radius of radial clearance of the spool valve	m
$P_{L(R)}$, P_E, $P_{A(B)}$	Servovalve pressures	Pa
P_S, P_T	Supply and tank pressures	Pa
$V_{L(R)}$	Left (right) chamber volume of the nozzle/flapper system	m^3
Re, Re_t	Reynolds number and transitional Reynolds number	
x_s, x_f, x_{f0}	Spool and flapper position, initial distance between the nozzle/flapper	m
x_{fG}, x_r	Position of flapper/armature gravity center, feedback spring deformation	m
x_i, x_{i0}	Total and initial underlap diameters of orifice i	m
x_0	Equivalent overlap diameter	m
l_t, l_r, l_f	Length of flexible tube, feedback spring, flapper	m
l_{re}, l_{fe}	Distance from flexible point of spring (flapper) to pivot center	m
θ_f	Angular position of the flapper/armature	rad
θ_i	Jet angular of orifice i	rad
K_m	Torque-motor gain	N.m/A
K_r,K_t	Feedback spring and flexible tube constant	N/m
E_t, E_r	Young's modulus of flexible tube and feedback spring	Pa
I_t, I_r	Moment of area of flexible tube and feedback spring	m^4
J_f	Flapper inertia	kg. m^2
m_s, m_f	Spool and flapper/armature mass	kg

B_f	Flapper viscous damping coefficient	Nm/(rad/s)
B_s	Spool viscous damping coefficient	N/(m/s)
i	Input current to the torque motor	A
k_t	Transitional constant	
k_I	Energy losses constant due to fluid inertia	m
v_P	Piston velocity	m/s
β	Compressibility of hydraulic oil	N/ m^2
ρ	Density of hydraulic oil	kg/ m^3
δ	Asymptote slope	
μ	Dynamic viscosity	Pa.s

7 REFERENCES

Dransfield, P.; Teo, M.K. (1979). Using bond graph in simulating an electro-hydraulic system. *Journal of the Franlin Institute, Vol. 308, n° 3, pp. 173-184.*

Kang, R.J.; Jiao, Z.X.; Mare J.C.; Shang, Y.X.; Wu, S. (2009). Nonlinear Block Diagram Model and Robust Control of Electro-hydrostatic Actuator. *Acta Aeronautica et Astronautica Sinica, Vol. 30, n° 3, pp. 518-525.*

Karnopp, D. (1972). Bond Graph models in fluid dynamic systems. *Journal of Dyn. Syst., Meas. and Control, Trans. ASME, Vol. 94, n° 3, pp. 222-229.*

Karnopp, D.C.; Rosenberg, R.C. (1975). *System Dynamics: a Unified Approach*. John Wiley & Sons, New York.

Kim, D.H.; Tsao, T.-C. (2000). A Linearized Electrohydraulic Servovalve Model for Valve Dynamics Sensitivity Analysis and Control System Design. *Journal of Dynamic Systems, Measurement, and Control, Vol. 122, pp. 179-187.*

Maré, J.C. (1996). Estimation of effective parameters and accurate simulation of hydraulic valves. *Proceeding of International Symposium on Fluid Machinery and Fluid Engineering, Beijing China, pp. 439-446.*

Merritt, H.E. (1967). *Hydraulic Control Systems*. John Wiley & Sons, New York.

Morse, A.C. (1963). *Electrohydraulic Servomechanisms*. McGRAW-HILL BOOK CO., New York.

Rabie, G.; Lebrun, M. (1981). Modélisation par Les Graphes à Liens et Simulation d'une Servovalve Electrohydraulique à Deux Etages. *R.A.I.R.O Automatique Systems Analysis and Control, vol. 15, n°2, pp. 97-129.*

Suzuki, K.; Nakamura, I.; Thoma, J.U. (1999). Pressure regulator valve by Bondgraph. *Simulation Practice and Theory, Vol. 7, pp. 603-611*.

Watton, J. (1987). The Effect of Drain Orifice Damping on the Performance Characteristics of a Servovalve Flapper /Nozzle Stage. *Journal of Dyn. Syst., Meas. and Control, Trans. ASME, Vol. 109, pp. 19-23.*

Yuan Q.H.; Li P.Y. (2002). An Experimental Study on the Use of Unstable Electrohydraulic Valves for Control. *Proceedings of the American Control Conference (ACC 2002), pp. 4843-4848.*